BOARD, PACKAGE AND DIE THICKNESS EFFECTS UNDER THERMAL CYCLING CONDITIONS

Jean-Paul Clech
EPSI Inc.
Montclair, NJ, USA
jpclech@aol.com

ABSTRACT

This paper presents a first-order model that enables the scaling of solder joint failure cycles for board and/or die or substrate thickness effects under thermal cycling conditions. The model also allows for the prediction of failure cycles for solder joints of double-sided, mirrored assemblies based on failure data for single-sided assemblies.

INTRODUCTION

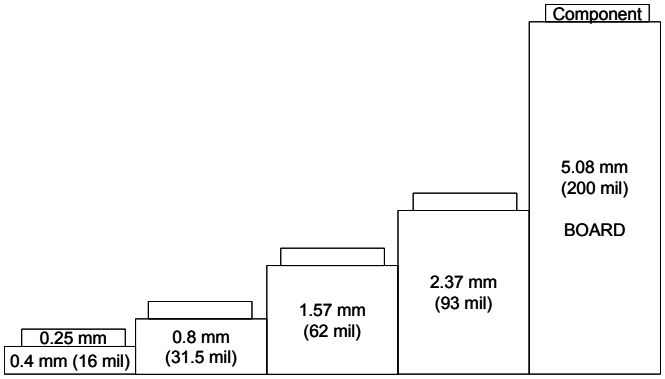

Figure 1: Board thickness in perspective, compared to a component that is 0.25 mm or 10 mil thick. Board and component cross-sections are approximately to scale in the thickness direction.

Product board thickness varies by one order of magnitude across the industry, from 0.4 mm (15.7 mil) or less to 5 mm (197 mil) or more. Boards and components are of comparable thickness or boards may be twenty times thicker than components (see Figure 1 for a 0.25 mm or 10 mil thick component on boards of thickness 0.4 to 5.08 mm). Boards that are used in Accelerated Thermal Cycling (ATC) often are 1 mm (39 mil), 1.575 mm (62 mil) or 2.36mm (93 mil) thick. Designers thus need to extrapolate solder joint life data from a given thickness to whatever product board thickness is required by end-user applications. However, solder joint life models in industry standards, e.g. IPC 9701 and IPC-SM785, assume that printed wiring boards are infinitely rigid and the existing models do not account for board thickness effects.

Under thermal cycling conditions, solder joint life can vary two to three times with board thickness. The prevalent trend is that solder joint life decreases with an increase in board thickness (e.g., Darveaux et al., 1998; Syed et al., 1999, Primavera, 1999; Lau et al., 2002; Vandevelde, 2004; Birzer et al, 2006; Ahmad et al., 2009; deVries, 2009). However, several datasets show very little change or a definite increase in solder joint life for leadless components mounted on thicker boards (Shi et al., 2004). These seemingly counter-intuitive trends are confirmed by finite element simulations of board assemblies under thermal cycling loads (Teng et al., 2002; Wu et al., 2014). To this author's knowledge, the physics behind these anomalous trends has not been elucidated. All of this leaves designers with a high level of uncertainty about the effect of board thickness on solder joint reliability.

The board thickness effect and the ability to predict life for mirrored assemblies vs. single-sided assemblies are already built-in in compact life prediction models developed for SnPb and lead-free assemblies (Clech et al., 1996, 2005, 2009). In this paper, simple formulas are extracted from these models to clarify the mechanics of board thickness effects and single vs. double-sided, mirrored assemblies. The formulas apply equally well to component or die thickness effects. The model is validated against thermal cycling test data for board thickness in the range 1 to 3.3 mm and component thickness from 0.2 to 3.7 mm.

"BOARD THICKNESS" MODEL

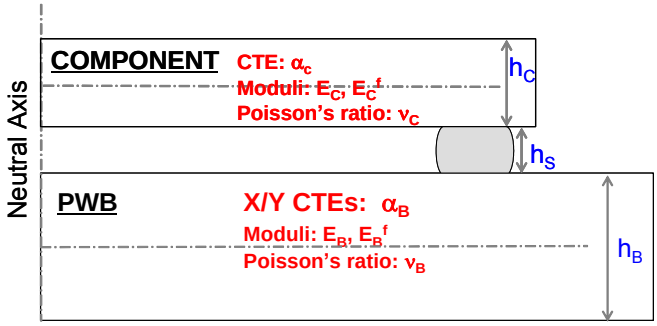

Figure 2: Board, component and assembly parameters that influence the "board thickness" effect on solder joint life.

Because of the mechanical coupling between components and Printed Wiring Boards (PWBs), the impact of board thickness on solder joint life cannot be treated in isolation. Instead, the analysis of board thickness effect considers the coupling of board and component stiffness, their relative values and other factors that might affect the compliance of the assembly during thermal cycling. The "board thickness" model that is presented in this paper accounts for eleven board, component and assembly parameters which are shown in Figure 2. The list of relevant parameters consists

of eight material properties, as well as the thickness of the board, the component and the solder joint.

From previous publications -- equation (4) in Clech, 1996, and equations (1) to (5) in Clech et al., 2009 -- the maximum cyclic strain energy density, ΔW_{max}, imparted to the outermost critical joints of a leadless assembly goes as:

$$\Delta W_{max} \propto K \cdot \Delta\alpha^2 \qquad (1)$$

where K is the assembly stiffness and $\Delta\alpha = |\alpha_B - \alpha_C|$ is the global CTE mismatch between board and component:

- α_B is the in-plane CTE of the board in the diagonal direction of the package, from the neutral axis of the component to the outermost critical joint.
- α_C is the in-plane CTE of the component in its diagonal direction, as measured or predicted on the solder joint side of the component.

Solder joint life follows an inverse relationship to cyclic strain energy density for standard SnPb and SAC assemblies (Clech, 1996, 2005). Thus, cycles to failure N_f go as:

$$N_f \propto 1/\left(K \cdot \Delta\alpha^2\right) \qquad (2)$$

Non-board related factors, including component size, temperature swing and dwell times, are left out of the above equations since the focus of this paper is on board thickness effects for a given component and a given thermal cycle.

The CTE mismatch is included in the analysis of board thickness effects since in-plane, effective CTEs of printed wiring boards are expected to change with board thickness. In-plane CTEs are strongly dependent on board contents, layer stack-up and thickness and material properties of the resin/fiber-glass system, pre-pregs, power and ground, and signal layers. Similarly, the board's effective moduli, in tension and in flexure, vary with board thickness. Their influence on solder joint reliability is captured by board rigidity factors within the assembly stiffness parameter K.

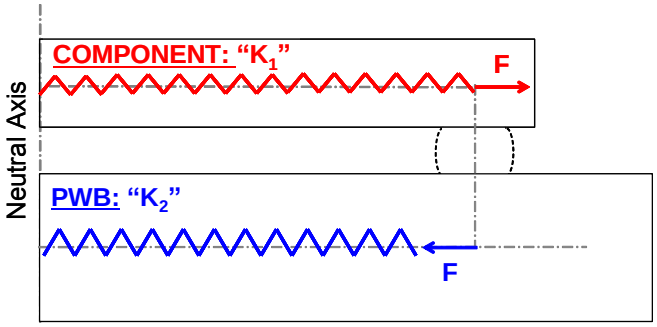

Figure 3: Schematic of solder joint shear forces, F, acting on the board and component neutral planes. The shear forces excite the in-plane tensile (or axial) stiffness of the component, K_1, and that of the board, K_2.

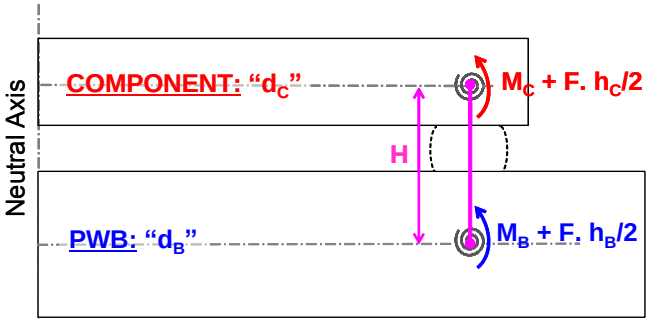

Figure 4: Schematic of solder joint moments (shown as curved arrows) acting on the board and component neutral planes. M_B and M_C are the moments at the solder joint to board and component interfaces, respectively. The moments excite the flexural rigidity of the component, d_c, and that of the board, d_B, as illustrated by spiral-like, rotational springs that operate in parallel. The composite link, H, that separates the neutral planes provides additional compliance to the assembly.

For single-sided assemblies, the assembly stiffness K is that of three springs in series (Clech, 1995, 1996):

$$\frac{1}{K} = \frac{1}{K_1} + \frac{1}{K_2} + \frac{1}{K_3} \qquad (3a)$$

- K_1 is the in-plane, tensile stiffness of a slice of the component of width the pitch P of the assembly:

$$K_1 = \frac{E_C h_C P}{L_D (1-\nu_C)} \qquad (3b)$$

As shown schematically in Figure 3, K_1 is excited by solder joint shear forces on the component side.

- K_2 is the in-plane tensile stiffness of a slice of the board of width the pitch P and subject to a tensile force at a distance L_D (or Distance to Neutral Point) from the neutral axis of the assembly[1]:

$$K_2 = \frac{2E_B h_B P}{L_D (1-\nu_B^2)} \qquad (3c)$$

As seen in Figure 3, K_2 is activated by solder joint shear forces from the board side.

- K_3 is a spring constant that accounts for bimetallic strip bending of the board to component assembly:

$$K_3 = (d_C + d_B)\frac{P}{L_D H^2} \qquad (3d)$$

[1] The formula for K_2 in Clech, 1996, had a typo whereby the Poisson ratio ν_B was not squared. The formula is being corrected here. The reader, and users of the SRS model, can verify that equation (3c) gives the same value of K_2 as in the stiffness validation example of Clech, 1996. The author is grateful to Jean-Baptiste Libot, Ph. D. student, SAGEM / ENIT / Université de Toulouse, for bringing this typo to his attention some eighteen years after publication.

where $H = \frac{h_C}{2} + h_S + \frac{h_B}{2}$ is the distance between the neutral plane of the board and that of the component. d_C and d_B are component and board flexural rigidity factors:

$$d_C = \frac{E_C^f h_C^3}{12(1-\nu_C)},\ d_B = \frac{E_B^f h_B^3}{6(1-\nu_B^2)}. \qquad (3e)$$

In the above equations, subscripts i = "C" and "B" are for component and board parameters, respectively. h_S is the solder joint height, h_C is the component thickness, h_B is the board thickness, ν_i's are Poisson's ratios, E_i's are Young's moduli in tension, E_i^f's are Young's moduli in flexure (superscript "f").

The stiffness K_3 of the bi-metallic assembly goes as the sum of board and component flexural rigidity factors, d_B and d_C. When the board thickness increases, d_B increases, making the assembly stiffer. At the same time, the length of the link H (Figure 4) from the neutral plane of the component to the neutral plane of the board increases. This makes the bi-metallic assembly more compliant and the stiffness K_3 decreases as per equation (3d). The changes in H and d_B go in opposite directions. Depending on the thickness of the component, that of the solder joint and the flexural rigidity of the component, d_C, the "H" factor may carry more weight, resulting in a lower value of the stiffness K_3 when the board thickness increases.

For double-sided, mirrored assemblies with identical components mounted back-to-back on the top and bottom sides of a board, K is obtained from the following equation (Clech, 1996):

$$\frac{1}{K} = \frac{1}{K_1} + \frac{1}{(K_2/2)} \qquad (4)$$

where K_1 and K_2 are given by the same formula (3b) and (3c) as for a single-sided assembly. The "1/K3" term has dropped out since, by symmetry, the mirrored assembly is not allowed to bend. The board stretching stiffness K_2 is halved since solder joint shear forces on each side of the board act on half the board thickness.

By combining equations (2) to (4), and dropping the non-board related factors, the "board thickness" model goes as:

$$N_f = F \cdot \frac{\frac{1-\upsilon_C}{E_C h_C} + \frac{1-\upsilon_B^2}{2E_B h_B} + \frac{H^2}{\frac{E_C^f h_C^3}{12(1-\upsilon_C)} + \frac{E_B^f h_B^3}{6(1-\upsilon_B^2)}}}{\Delta\alpha^2} \qquad (5a)$$

for single-sided assemblies.

or $$N_f = F \cdot \frac{\frac{1-\upsilon_C}{E_C h_C} + \frac{1-\upsilon_B^2}{E_B h_B}}{\Delta\alpha^2} \qquad (5b)$$

for mirrored assemblies.

The calibration factor "F" is a proportionality constant for a given component and a given thermal cycle. The same constant "F" appears in (5a) and (5b) because the same fatigue law (equation (2)) applies to single-sided and mirrored assemblies when the same solder joint composition is used on both sides of the board. Theoretically, it only takes one thermal cycling test using one type of test vehicle with a given board thickness to obtain the empirical factor F from either equation (5a) or (5b). One can then predict solder joint life for boards of different thickness (and known CTEs and moduli) or for another assembly configuration, either single-sided or a mirrored assembly.

Even though equations (5a) and (5b) are intended to capture the board thickness effect, the model applies equally well to the component thickness effect by symmetry. This latter version of the model is excercised later on in the paper in application examples looking at the effect of bare die or CBGA substrate thickness on solder joint reliability.

SOLDER JOINT LIFE VS. COMPLIANCE FACTORS

The life equations (5a) and (5b) can be rewritten as follows. For single-sided assemblies:

$$N_f = N_1 + N_2 + N_3 \qquad (6a)$$

or $$N_f = \frac{F}{\Delta\alpha^2} \cdot (C_1 + C_2 + C_3) \qquad (6b)$$

where: $$N_1 = \frac{F}{\Delta\alpha^2} \cdot \frac{1-\upsilon_C}{E_C h_C} \qquad (6c)$$

$$N_2 = \frac{F}{\Delta\alpha^2} \cdot \frac{1-\upsilon_B^2}{2E_B h_B} \qquad (6d)$$

$$N_3 = \frac{F}{\Delta\alpha^2} \cdot \frac{H^2}{\frac{E_C^f h_C^3}{12(1-\upsilon_C)} + \frac{E_B^f h_B^3}{6(1-\upsilon_B^2)}} \qquad (6e)$$

- N_1 is the part of life that is controlled by the axial compliance of the component: $C_1 = \frac{1-\upsilon_C}{E_C h_C}$.
- N_2 is the part of life that is determined by the axial compliance of the board: $C_2 = \frac{1-\upsilon_B^2}{2E_B h_B}$.

- N_3 is the part of life that is controlled by the bending compliance of the bimetallic strip assembly of the board and component: $C_3 = \dfrac{H^2}{\dfrac{E_C^f h_C^3}{12(1-\upsilon_C)} + \dfrac{E_B^f h_B^3}{6(1-\upsilon_B^2)}}$.

For double-sided assemblies:

$$N_f = N_1 + N_2 \quad (7a)$$

or $$N_f = \frac{F}{\Delta\alpha^2} \cdot (C_1 + C_{2M}) \quad (7b)$$

where:

$$N_1 = \frac{F}{\Delta\alpha^2} \cdot \frac{1-\upsilon_C}{E_C h_C} \quad (7c)$$

$$N_2 = \frac{F}{\Delta\alpha^2} \cdot \frac{1-\upsilon_B^2}{E_B h_B} \quad (7d)$$

Note that, in mirrored assemblies, the axial compliance of the board: $C_{2M} = \dfrac{1-\upsilon_B^2}{E_B h_B}$ is twice as much as the board axial compliance C_2 in a single-sided assembly.

The break-down of solder joint life as per equations (6a) and (7a) helps identify which compliance factor has a dominant effect on assembly reliability.

BOARD THICKNESS EFFECT IN SINGLE-SIDED ASSEMBLIES

The first application example is that of a HiTCE CBGA on FR-4 boards, after an experiment by Shih et al., 2004. The board thickness was 62, 93 or 130 mil with measured X- and Y- direction CTEs and Young's moduli from Tables 2A and 2B in Shi et al., 2004. Figure 5 is a schematic of the three board assembly cross-sections, with board, solder attach and component substrate thickness approximately to scale in the vertical direction. Dimensions and material properties of interest are summarized in Figure 5. The effective board CTEs in the diagonal direction of the square CBGA package are calculated as the average of the measured X and Y CTEs in the component mounting areas. Solder joint thickness (0.41 mm or 16 mil) is from a related publication by Shih et al., 2005. The HiTCE substrate data and properties are averaged values based on measurements reported by end-users and substrate suppliers (Pendse et al., 2000; Dai et al., 2005; Shih et al., 2005).

From Figure 5, the effective CTE mismatches between board and component are 4.5, 4.45 and 7.35 ppm/ºC for board thickness of 62, 93 and 130 mil, respectively. While the 62 and 93 mil board assemblies have similar mismatches, the CTE mismatch of the 130 mil board test vehicles is 1.65 times larger. The largest difference in board modulus is 23 vs. 30 GPa (a 30% difference) for 93 mil boards vs. 130 mil boards. The experiment of Shi et al., 2004, clearly shows that the board thickness effect is not just about board thickness. Instead, the confounding influence of board CTEs and moduli has to be accounted for in the interpretation of "board thickness" test results.

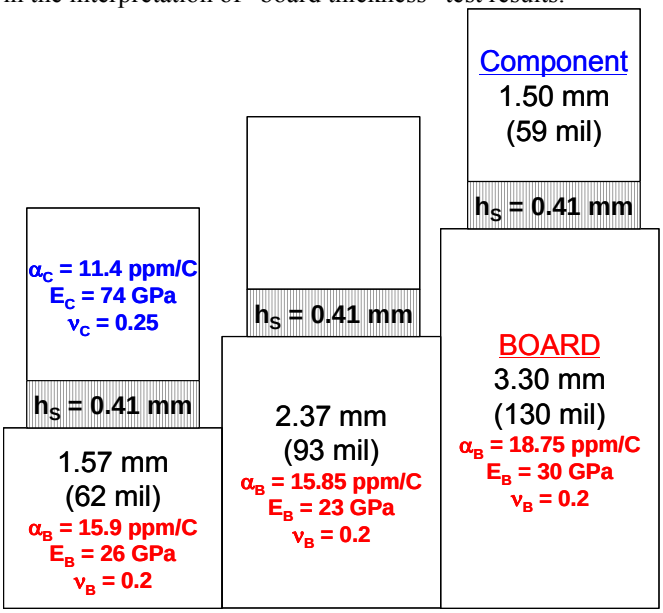

Figure 5: Board and component thickness – approximately on the same scale in the vertical direction -- in Shih et al.'s 2004 experiment. Component properties are shown for a HiTCE CBGA component. Test vehicle board thickness are: 62, 93 and 130 mil. Board in-plane CTEs are given in the diagonal direction of the square CBGAs.

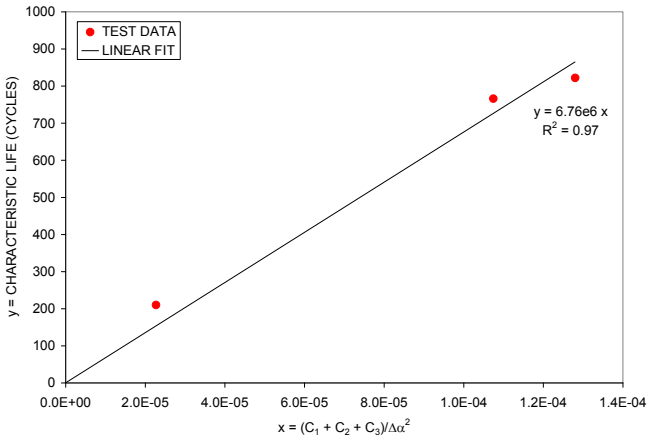

Figure 6: Linear fit of single-sided HiTCE CBGA test data to equation (6b) of board thickness model. The slope of the linear trend line with a zero intercept gives the empirical factor F in equations (5a) and (6b). Mixed units on the x-axis are: $[\text{MPa} \cdot \text{mil} \cdot (\text{ppm/ºC})^2]^{-1}$.

The model is fit to the test data in two steps. First, the empirical factor F is obtained by calculating the compliance factors C_1, C_2 and C_3 and plotting the test results (i.e. the characteristic lives for the three board thickness) vs. the right hand-side of equation (6b). The slope of the linear trend line with a zero intercept through the data points (Figure 6) gives a best estimate of F. The goodness of fit of

the model is assessed by the correlation coefficient R^2 = 0.97, which is close to 1. Next, we plot the data and the model curves (characteristic lives vs. board thickness as per equation 5a) as shown in Figure 7. The three model lines are plotted for fixed values of the board CTE and modulus as per the legend of the chart, using the 62, 93 and 130 mil board properties from Shih et al.'s experiment.

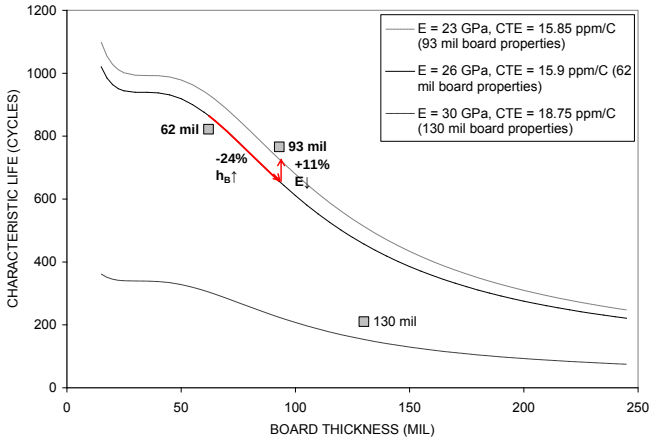

Figure 7: Plot of characteristic lives vs. board thickness as per equation 5a, and single-sided HiTCE CBGA test data (square symbols) in Shi et al., 2004. Plotted lines are for fixed values of the board CTE and modulus for the three test board thickness in Shi et al.'s experiment.

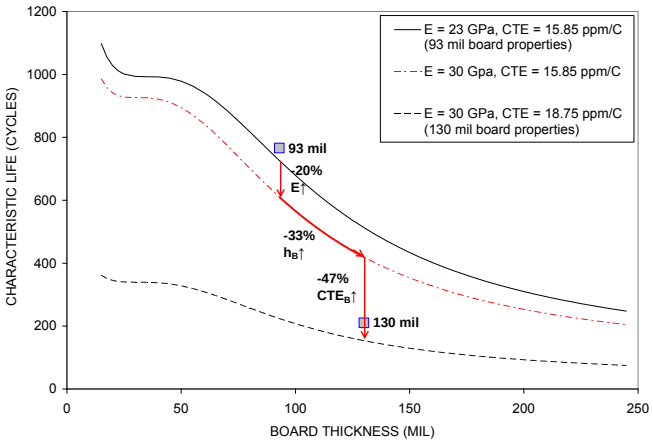

Figure 8: Plot of characteristic lives vs. board thickness for "93 mil" and "130 mil" board properties, with intermediate line being plotted for the same CTE as in the top line ("93 mil" board properties) but with modulus being increased from 23 to 30 GPa.

Going from 62 to 93 mil, the board thickness increases by 1.5 times, i.e. by a large amount. In Shih's accelerated thermal cycle, the characteristic life decreases by a small amount, 7%, from 822 to 766 cycles. The board diagonal CTEs are very close (15.9 vs. 15.85 ppm/ºC), thus, the board thickness effect is not confounded with changes in CTEs. Following the red arrowed lines in Figure 7, the model shows that, had the board modulus not changed, life would have decreased by about 24% due to the increase in board thickness. However, due to a decrease in board modulus (from 26 to 23 GPa), the latter life increases by 11%. About half of the life loss associated with the increase in board thickness is compensated by the lower modulus of the 93 mil board. The overall loss of life that is predicted by the model, 13%, is small and consistent with the 7% loss of life in test. The latter is a median loss of life, which could be more (or less) since the median values of characteristic lives in thermal cycling are estimated with a typical uncertainty of 10 to 25% based on confidence bands at the 90 to 95% level.

Figure 8 is similar to Figure 7, except that the curve with "62 mil" board properties has been removed. Instead, another curve has been added in (red dashed line) for a hypothetical board with the same CTE as that of the "93 mil" board but with its modulus changed from 23 to 30 GPa. By following the path of the three red-arrows in Figure 8, the loss of life due to the increase in board thickness from 93 to 130 mil under test conditions can be broken down into three parts, showing the effect of the change in modulus, the increase in thickness per se and the change in the board CTE. The first arrow in between the top two lines gives the loss of life due to the increase in modulus alone. For a board thickness of 93 mil, when the modulus increases from 23 to 30 GPa (with no change in board CTE), the life loss is 20% of the total life loss when comparing the life data for the 93 and 130 mil boards. The second arrow follows the intermediate hypothetical curve from 93 to 130 mil. Due to the increase in board thickness alone (with no change in board properties), the corresponding loss of life is about 33% of the total life loss in test. Last, when following the vertical arrow between the bottom two curves for 130 mil thick boards, the board modulus does not change (30 GPa) but the board CTE increases from 15.85 to 18.75 ppm/ºC. The corresponding loss of solder joint life is 47% of the total loss of life in test. That is, when going from 93 to 130 mil thick boards, about half of the drop in life is attributed to the increase in board CTE. Clearly, the board thickness effect is confounded with changes in board properties, CTE and modulus.

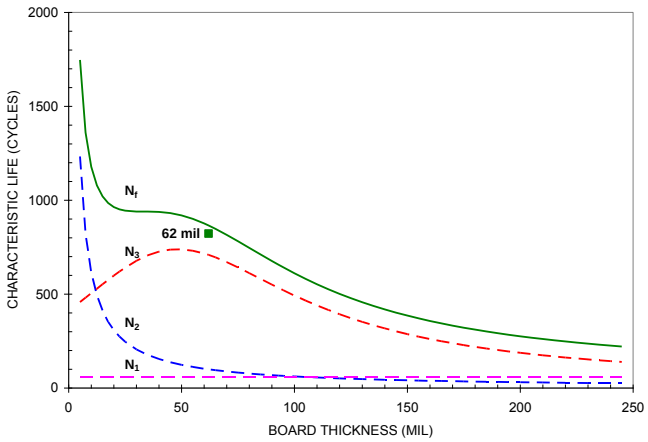

Figure 9: Plot of life vs. board thickness for "62 mil" board properties, and break-down of life curve by compliance factors (as per equation (6a)).

The middle curve of Figure 7 with "62 mil" board properties is re-plotted in Figure 9 and broken down by compliance factors as per equation (6a).

- The "N_1" part of life, which represents the contribution of the axial compliance of the component to solder joint life, N_f, is constant and fairly low. This is not surprising as the 59 mil thick HiTCE CBGA is a rather stiff element in tension.
- The "N_2" curve, which is associated with the in-plane, axial compliance of the board follows an inverse relationship with board thickness. Past a board thickness of 100 mil, N_2 is less than N_1, which means that the board is as stiff as or stiffer than the component under in-plane tensile loads, and the N_2 part of the solder joint life becomes smaller and smaller. On the other hand, for very thin boards, 10 mil or less in thickness in the upper left corner of the plot, N_2 becomes the dominant factor. That is, for very thin boards or flex substrates, the axial compliance of the board becomes the life controlling factor.
- The "N_3" curve in Figure 7 represents the part of life that is associated with bi-metallic strip bending of the assembly. For boards thicker than 12 mil in the present HiTCE CBGA example, N_3 is larger than N_1 and N_2. and the bi-metallic strip bending stiffness becomes the life controlling factor. This is consistent with strain measurements by Hall (1984) who showed that board and component bending are the primary deformation mode of leadless ceramic chip carriers on PWBs during temperature cycling.

The "N_3" curve shows a maximum life for a board thickness of 50 mil. The peak in the N_3 curve explains the intermediate plateau in the total life curve (N_f vs. board thickness). Below 50 mil, N_3 increases as the board thickness increases. At 50 mil, the board flexural rigidity, d_B, is 1/3 of the component flexural rigidity, d_C. At 33 mil, d_B is less than $1/10^{th}$ of d_C. Below 50 mil, the effect of the H factor is greater than that of the board plus component flexural rigidity because the board rigidity factor d_B is much smaller than the component rigidity factor d_C. The compliance C_3 of the bi-metallic strip assembly and the life N_3 go up as the board thickness increases. This is consistent with life increases that have been reported for some components when board thickness increases (Shih et al., 2004; Wu et al., 2014). For boards thicker than 50 mil, N_3 decreases in a monotonous manner as the board thickness increases. In that region, the board flexural rigidity becomes the controlling factor, more so than the separation H between the board and component neutral planes.

BOARD THICKNESS EFFECT IN DOUBLE-SIDED, MIRRORED ASSEMBLIES

Figure 10 shows the plot of test results and life predictions for the mirrored HiTCE CBGA assemblies of Shih et al., 2004. The test data was split into two sets of failure statistics, one for each side of the board. We used the failure statistics from the side of test boards that gave the lowest cycles to failure since this would be the worst case scenario for reliability of a double-sided module. The curves of life vs. board thickness in Figure 10 for a given pair of board properties (modulus and CTE) are graphed as per equation (5b) for mirrored assemblies, using the same empirical factor F as for single-sided assemblies. For the 62 and 93 mil thick test boards, the life predictions are off the test results by 13% and 8%, respectively. For the 130 mil test board, the difference between the predicted life and the test data is 28%. Given that the empirical factor F was obtained from the failure data for single-sided test vehicles, the life predictions for mirrored assemblies are in good agreement with test results.

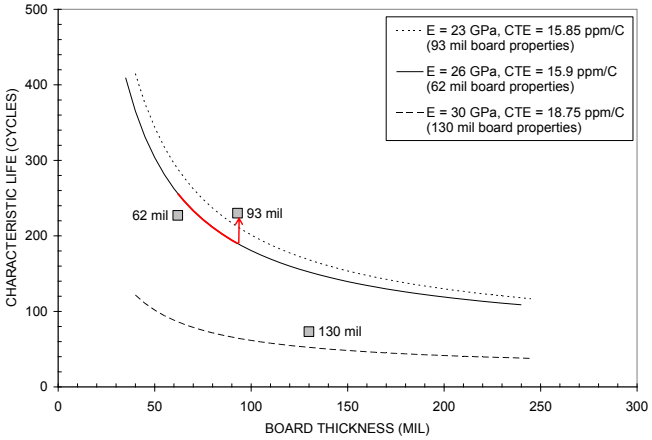

Figure 10: Plot of characteristic lives vs. board thickness as per equation 5a for mirrored HiTCE CBGA assemblies. Plotted lines are for fixed values of the board CTE and modulus for the three board thickness in Shi's experiment. Test data (square symbols) are from Shi et al., 2004.

The trends of test data for the mirrored HiTCE CBGA assemblies are similar to those of single-sided assemblies, and the effect of board thickness on failure cycles is interpreted in similar terms, including the confounding influence of board thickness, CTE and modulus. Of particular interest are the 62 mil vs. 93 mil test results, with failure cycles for the latter being slightly better than for the thinner board. The difference is not statistically significant given the usual spread of confidence bands around characteristic lives. Part of the difference in the 62 mil vs. 93 mil test results is explained by the lower modulus of the 93 mil board. This can be seen by following the red path in Figure 10, where the predicted decrease in life due to increase in thickness is partially compensated by the lower modulus of the 93 mil board.

Next, we look at the ratio of cyclic lives for single-sided boards vs. double-sided, mirrored assemblies. The life curves and test results for mirrored and single-sided assemblies are re-plotted in Figure 11 for boards with "62 mil" properties (E = 26 GPa; CTE = 15.9 ppm/°C). The life ratio for single-sided over mirrored assemblies is plotted on the secondary axis -- to the right of the chart -- as a function of board thickness. This ratio varies by a large factor with

board thickness. In the range 50 to 130 mil, the life ratio is greater than 3 and peaks at 3.5 for an 80 mil thickness. For thicker boards, the life ratio decreases in a monotonic way, down to almost 2 when the thickness is 240 mil.

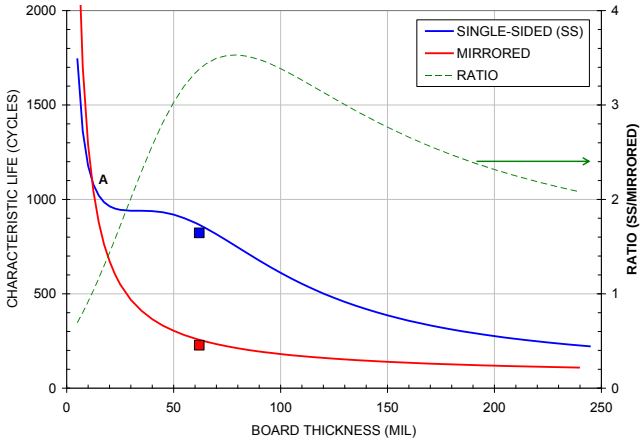

Figure 11: Comparison of failure cycles vs. board thickness for single-sided and mirrored HiTCE CBGA assemblies, using "62 mil" board properties. The corresponding ratio of lives, "single-sided" / "mirrored" (green dashed line) is shown on the secondary vertical axis. Square symbols are test data from Shi et al., 2004.

For very thin boards, less than 12.5 mil or flex circuits, the life ratio drops below one. This is counter to the prevalent trend for thicker boards, whereby solder joint life of mirrored assemblies is less than that of single-sided assemblies (Juso et al., 1998; Ghaffarian, 1999; Primavera, 2003; Shih et al., 2004). As seen in Figure 11, the life ratio is less than 1 to the left of point A where the two life curves intersect. As discussed earlier, in that region of the chart for very thin, single-sided boards, the axial compliance of the board is the life controlling factor. That is, the solder joint life N_f(single-sided) goes as N_2 in equation (6d):

$$N_f(\text{single-sided}) \approx \frac{F}{\Delta\alpha^2}\cdot\frac{1-\upsilon_B^2}{2E_B h_B} \qquad (8a)$$

For mirrored assemblies on very thin boards, the solder joint life N_f(mirrored) goes as N_2 in equation (7d):

$$N_f(\text{mirrored}) \approx \frac{F}{\Delta\alpha^2}\cdot\frac{1-\upsilon_B^2}{E_B h_B} \qquad (8b)$$

From the ratio of equations 8a and 8b, when h_B is very small, the life ratio of "single-sided" over "mirrored" assemblies goes down to 1/2, obviously less than 1. Physically, since the axial compliance of the board is the life controlling factor, the solder joint shear forces on one side of the mirrored assembly work against one half of the board thickness whereas, in a single-sided assembly, the solder joint shear forces work harder against the full board thickness. To this author's knowledge, no complete test data, including effective modulus and in-plane CTEs of very thin boards or flex circuits, is available in the public domain to test the validity of the above prediction.

DIE THICKNESS EFFECT IN WLCSP ASSEMBLY

This next section looks at the applicability of the model to die thickness effects in bare chip assemblies without underfill.

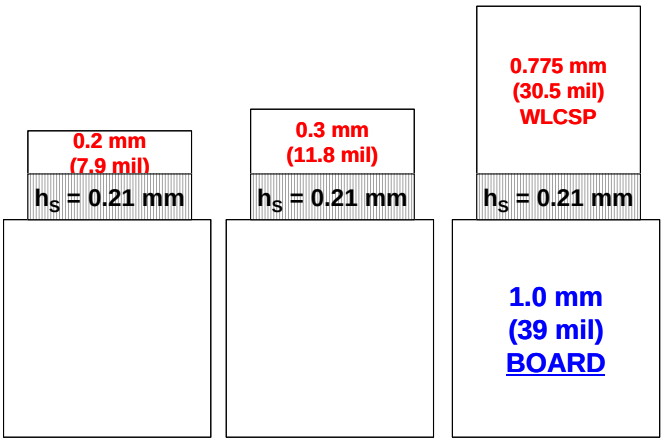

Figure 12: Board and chip thickness in perspective (approximately on the same scale in the vertical direction) in Chen's 2010 experiment. The test variable is the chip thickness: 0.2, 0.3 and 0.775 mm.

The test vehicle is a lead-free, single-sided Wafer Level Chip Scale Package (WLCSP) with a fixed board thickness of 1 mm and component thickness: 0.2, 0.3 or 0.775 mm (i.e. 7.9, 11.8 or 30.5 mil) (Figure12) from an experiment by Chen, 2010. Material properties and thermal cycling data that are used in the model are from tables II and VIII, respectively, in Chen, 2010. The WLCSP is a silicon die with a very thin polyimide layer (5 μm cured thickness) on the active side of the chip, which is thought to have a very small effect on the effective modulus and CTE of the package. In the component thickness model, the WLCSP is treated as a bare silicon die. The CTE mismatch between board and component is not a variable in Chen's experiment and can be left out of the thickness model equations (5a, 6a).

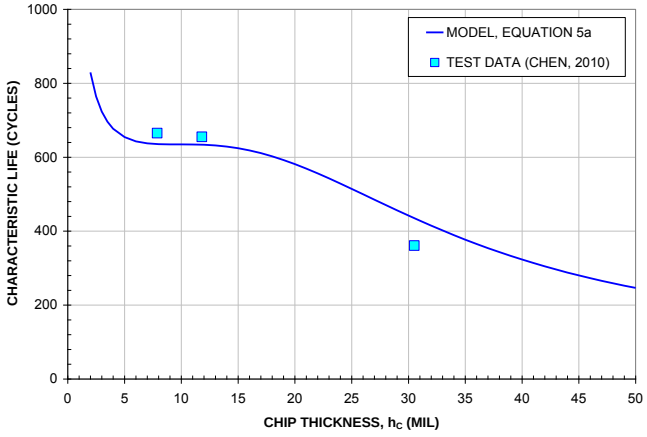

Figure 13: Plot of characteristic lives vs. chip thickness as per equation 5a, and WLCSP test data (square symbols) in Chen's 2010 experiment.

The model (equation 5a) is fitted to the test data as characteristic life vs. chip thickness (N_f vs. h_C). The results

are plotted in Figure 13. The test cycles to failure are off the model by -15% to +4%. The data for the thinner chips (0.2 and 0.3 mm or 7.9 and 11.8 mil, a 50% difference), for which the characteristic lives are very close (665 and 655 cycles, respectively), fall in the intermediate plateau or shoulder area of the plot. This gives further support to the model (equation 5a) and to the overall shape of the predictive curve (N_f vs. thickness) for single-sided assemblies.

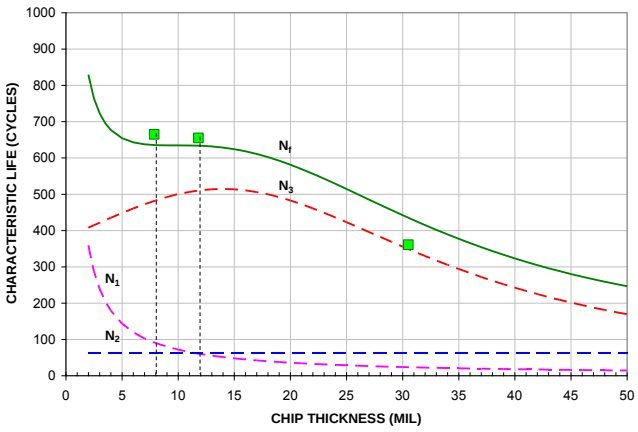

Figure 14: Plot of life vs. chip thickness and break-down of life curve by compliance factors (as per equation (6a)).

The life vs. chip thickness curve is re-plotted in Figure 14, showing the break-down of life into three parts: N_1, N_2 and N_3 according to compliance factors and equations 6a to 6e.

- The N_1 curve relates to the part of life that is controlled by the axial compliance of the die. As chip thickness decreases, say below 5 mil, N_1 becomes a larger part of the total life N_f. In that range, the axial compliance of the chip becomes a more and more significant contributor to solder joint life. For thicker chips, say thicker than 12 to 15 mil, N_1 becomes very small. These thicker chips are very stiff in tension and their axial compliance does not provide for stress relief in solder joints.
- The N_2 curve represents the contribution of the board compliance to life. The curve is flat since the board thickness is not a variable in Chen's experiment. Overall, the board axial compliance is a small contributor to solder joint life.
- N_3, the part of life that is associated with bi-metallic strip bending of the assembly is always greater than N_1 and N_2 for the range of thickness in Figure 14. The N_3 curve peaks for a chip thickness of 15 mil. For the two test chips to the left of that peak, 7.9 and 11.8 mil thick, N_3 increases with chip thickness because the H factor has a stronger effect on life than the sum of the board and component flexural rigidities. At the same time, N_1, the part of life associated with the axial compliance of the chip decreases by a similar amount. Since the N2 curve is flat, the total life $N_1 + N_2 + N_3$ does not change much, as observed in test (Chen, 2010).

BOARD, SUBSTRATE THICKNESS & DNP EFFECT

As a last example, we apply the model to a 1mm pitch, lead-free CBGA where both the board and ceramic substrate thickness change as well as the size of the component (see Table 4.1 in Farooq et al, 2003). In this experiment, the 42 mm square CBGAs had a substrate thickness of 1.5, 2.55 or 3.70 mm and were mounted on 60 mil (1.52 mm) thick FR-4 boards. The 32 mm square CBGAs had a substrate thickness of 1.50 or 2.40 mm and were mounted on 70 mil (1.78 mm) thick FR-4 boards. The matrix of board and substrate thickness is illustrated by the schematics of assembly cross-sections in Figure 15.

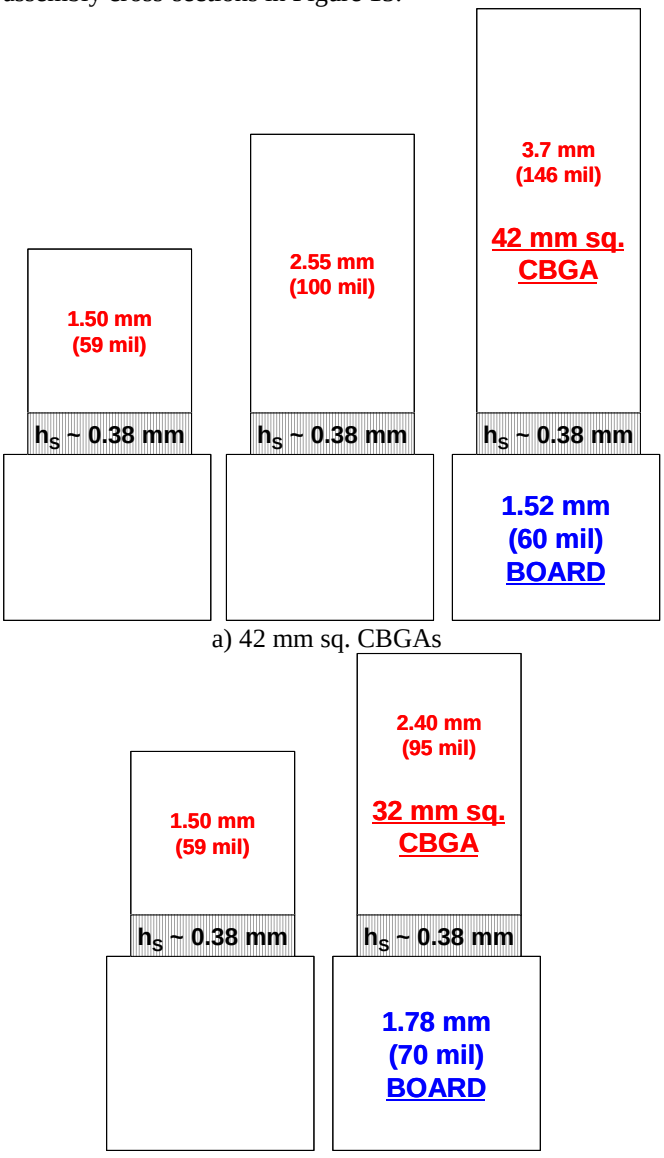

Figure 15: Board and CBGA substrate thickness in perspective (approximately on the same scale in the vertical direction) in Farooq et al.'s 2003 experiment. The test variables are the substrate thickness, the board thickness (60 and 70 mil) and the package size (32 and 42 mm sq.).

The 42 mm square CBGA packages are 31% larger on the side than 32 mm square CBGAs. From Coffin-Manson type

of relationships (IPC-9701), the size effect is squared and we would expect a life ratio of $1.31^2 = 1.72$. Comparing median test cycles to failure (1st and 4th rows in Table 4.1 of Farooq et al., 2003) for the two package sizes with 1.50 mm thick substrates, the life ratio is 1860 cycles / 1628 cycles = 1.14. Clearly, there is a discrepancy between test results and IPC standards predictions. To address this issue, we add the component size -- or Distance to Neutral Point (DNP) effect – to the board thickness model.

Going back to equation (1), and restoring the DNP factor, L_D, into the formulation of the maximum cyclic strain energy density (Clech, 1996; Clech et al., 2009), we get:

$$\Delta W_{max} \propto K \cdot (L_D \cdot \Delta\alpha)^2 \qquad (9)$$

From (3a-e) and (4), the assembly stiffness K goes as $1/L_D$. Assuming that the assembly pitch P does not change (an important assumption and an intentional restriction of the present model), the solder joint life equations (5a) and (5b) become:

$$N_f = F \cdot \frac{\dfrac{1-\upsilon_C}{E_C h_C} + \dfrac{1-\upsilon_B^2}{2E_B h_B} + \dfrac{H^2}{\dfrac{E_C^f h_C^3}{12(1-\upsilon_C)} + \dfrac{E_B^f h_B^3}{6(1-\upsilon_B^2)}}}{L_D.\Delta\alpha^2} \qquad (10a)$$

for single-sided assemblies.

or $$N_f = F \cdot \frac{\dfrac{1-\upsilon_C}{E_C h_C} + \dfrac{1-\upsilon_B^2}{E_B h_B}}{L_D.\Delta\alpha^2} \qquad (10b)$$

for mirrored assemblies.

Equations (10a) and (10b) are similar to (5a) and (5b) with an added $1/L_D$ multiplicative factor for the DNP effect on cycles to failure. This is at a departure from Coffin-Manson relationships (IPC-9701) where the DNP effect is almost squared. To this author's knowledge, the N_f vs. $1/DNP^2$ relationship in IPC-9701 has not been thoroughly tested. Instead, most life vs. DNP datasets examined by the author show a power-law trend with exponents below the -2 exponent of Coffin-Manson type of models, in absolute value. They often are close to -1 (Clech, 2015). The main reason for this, according to the above model, is the compliance or elasticity of the assembly, with the assembly stiffness K having an inverse relationship to the maximum DNP. The need to revisit the formulation of the DNP effect in Coffin-Manson type of models will be discussed in more details in a future publication. On the other hand, the CTE mismatch factor remains squared: $N_f \sim 1 / \Delta\alpha^2$ in equations (5a-b) and (10a-b), in agreement with IPC-9701 and as further validated by test data in Clech, 2015 & 2016.

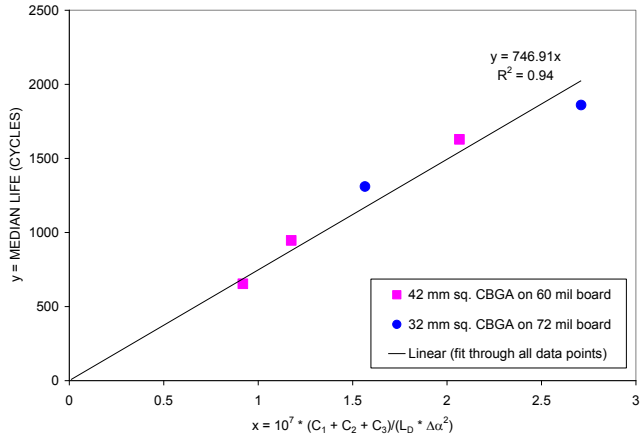

Figure 16: Linear fit of single-sided CBGA test data to equation (10a) of DNP-modified, board thickness model. The slope of the linear trend line with a zero intercept gives the empirical factor F in equation (10a). Mixed units on the x-axis are: [MPa . mil . (ppm/ºC)^2 . mm]$^{-1}$.

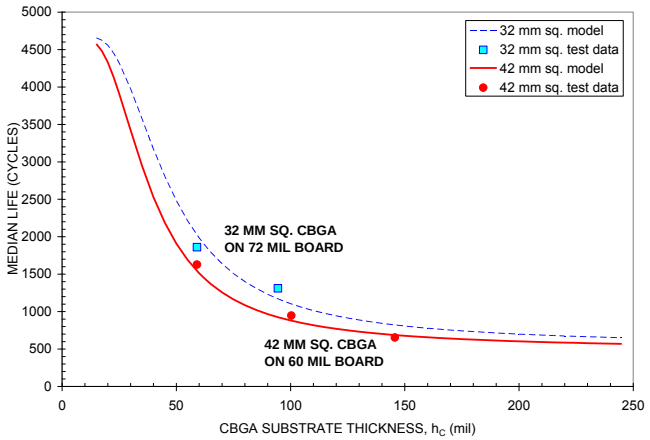

Figure 17: Plot of median lives vs. CBGA substrate thickness -- as per equation 10a – for two CBGA sizes (32 and 42 mm sq.). The test data points are for different substrate thickness in Farooq et al.'s 2003 experiment.

Equation (10a) accounts for the three test variables in the Farooq et al., 2003 experiment: the board thickness, h_B, the CBGA substrate thickness, h_C, and the maximum or critical DNP, L_D. The empirical factor F is obtained by fitting equation (10a) to the test data as was done earlier in the HiTCE CBGA example (see Figure 16). The fit between the model and the Farooq CBGA test data gives a correlation coefficient $R^2 = 0.94$. This indicates that, for a given pitch and stand-off height, the model does a good job of capturing the effects of the test variables in the Farooq et al.'s 2003 experiment., component size or maximum DNP) included.

Figure 17 shows plots of median lives vs. substrate thickness for the two CBGA component sizes (32 and 42 mm sq.). The difference between calculated lives and test data is 11% at most, which is another measure of the goodness-of-fit between the model and the data. It is noteworthy that it takes a single empirical constant (the

calibration factor F) to fit the two curves to the two datasets (32 and 42 mm sq.). The five data points are located in the elbow areas of the curves, away from the shoulder in the top left side of Figure 17. The life curves drop off steeply in between these two areas, suggesting that solder joint reliability of these CBGA assemblies can be further improved by going to thinner substrates.

DISCUSSION

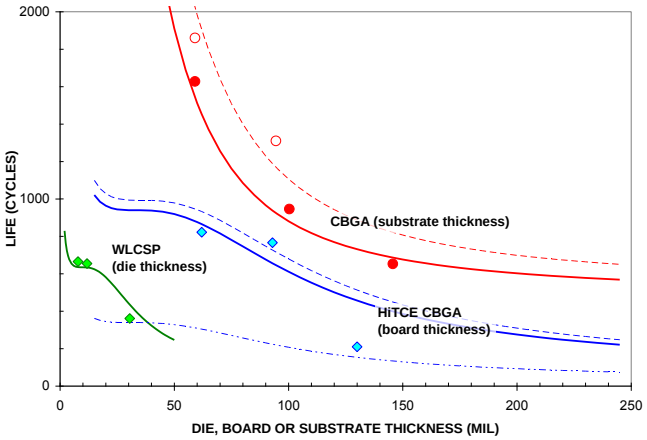

Figure 18: Plot of life vs. thickness of die, board or substrate in single-sided assemblies of application examples.

To put things in perspective in terms of the shape of life vs. thickness curves for single-sided assemblies, the results of the prior application examples are all plotted in one chart (Figure 18). The range of board thickness that is covered in the application examples is: 39 to 130 mil (1 to 3.3 mm). The range of component thickness is: 0.2 mm to 3.7 mm.

The WLCSP experiment of Chen, 2010 includes two thin chip data points that fit the shoulder area of the model curve. The HiTCE CBGA experiment of Shih et al.. 2004 includes two data points (62 and 93 mil boards) that are in the upper arm section of the curves, that is, in the descending parts of the curves to the right of the shoulder areas. The CBGA data points in the experiment of Farooq et al., 2003 fall in the elbow areas of the life vs. substrate thickness curves. That is, different sections of the curves are validated by different experiments using dissimilar boards and components. The only section of the curves for which relevant data could not be found is to the left of the shoulder area. This would be the area of solder joint life for very thin chip or flex circuit assemblies where, from previous discussions, the axial compliance of the chip or that of the flex substrate becomes the controlling factor.

CONCLUSIONS

1. A first-order design-for-reliability tool / model has been developed that captures the impact of board and/or component thickness on solder joint reliability under thermal cycling conditions.
2. The tool allows for scaling of failure cycles from one board thickness to another, or from one assembly configuration to another (single-sided or mirrored).
3. Solder joint life under thermal cycling conditions goes as the inverse of the assembly stiffness.
4. The model has been validated against thermal cycling results for 1 to 3.3 mm thick test boards and 0.2 to 3.7 mm thick components.
5. The model also accounts for the global CTE mismatch between board and component, as well as the component size (DNP) effect.
6. Other important parameters, such as stand-off height, assembly pitch and pad sizes are being added to the model (to be presented in a future publication).
7. The model is algebraic and is easily implemented in a spreadsheet. This allows for quick assessments of the relative impact of changes in design parameters and material properties on solder joint reliability, independent of soft solder compositions.
8. The board thickness effect is confounded with concurrent changes in in-plane moduli and CTEs. The interpretation of thermal cycling test results and the extrapolation of test data to field conditions rely heavily on realistic estimates, or better, measurements of board properties. In our updated survey of test board properties from multiple sources (Figure 19), board modulus is anywhere in the range 10 to 30 GPa and in-plane CTEs are in the range 12 to 21 ppm/ºC. Effective board properties vary widely and cannot be assigned randomly when entered into reliability models.

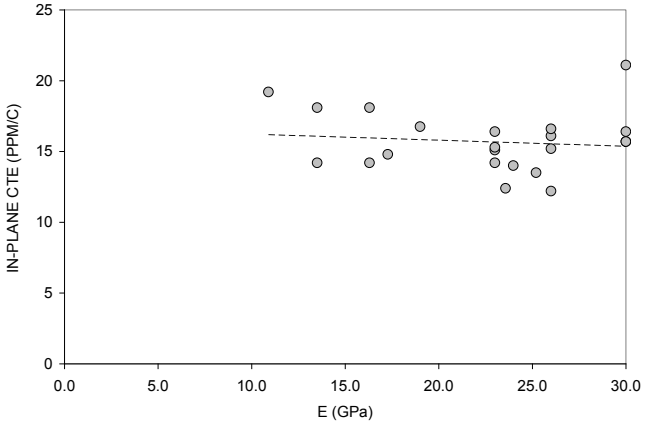

Figure 19: Updated survey of FR-4 test board properties at room temperature. Young's modulus, E, is on the horizontal axis; in-plane CTEs are on the vertical axis.

9. The stiffness or strength-of-materials approach, which is the foundation of the board and component thickness model, provides qualitative and quantitative insight into controlling parameters and competing factors: a) the board and component stiffness in flexure and under axial loading; b) the distance H that separates the neutral planes of the board and of the component. The latter increases the compliance of thicker board assemblies, a potential factor in some thick boards having longer solder joint lives than thin board assemblies as observed in accelerated thermal cycling and finite element simulations (Teng et al., 2002; Shih et al., 2004; Wu et al., 2014). These situations were not

modeled in this paper because relevant board and package material properties were not available.

ACKNOWLEDGEMENTS

The author thanks Jian Miremadi and Rocky Shih of the Hewlett-Packard Company for discussions on components of the HP board thickness experiment and related matters.

REFERENCES

- Ahmad, M., Xie, W., Liu, K-C., Xue, J. and Towne, D., "Parametric acceleration transforms for lead-free solder joint reliability under thermal cycling conditions", IEEE, Proceedings, ECTC 2009.
- Birzer, C., Stoeckl, S., Schuetz, G. and Fink, M., "Reliability investigations of leadless QFN packages until end-of-life with application-specific board-level stress tests", IEEE, Proceedings, ECTC 2006.
- Chen, K. M., "Lead-free solder material and chip thickness impact on board-level reliability for low-K WLCSP", *IEEE Transactions On Advanced Packaging*, Vol. 33, No. 2, May 2010, pp. 340-347.
- Clech, J-P., Solder Joint Mechanics, EPSI Inc., 1995.
- Clech, J-P., "Solder Reliability Solutions: a PC-based design-for-reliability tool", Proceedings, Surface Mount International Conference (SMTA), 1996, pp. 136-151.
- Clech, J-P., "Acceleration Factors and Thermal Cycling Test Efficiency for Lead-Free Sn-Ag-Cu Assemblies", Proceedings, SMTA International Conference, Chicago, Illinois, September 25 -29, 2005.
- Clech, J-P., Henshall, G. and Miremadi, J. "Closed-form, strain-energy based acceleration factors for thermal cycling of lead-free assemblies", Proceedings, SMTA International Conference, Oct. 4-8, 2009, San Diego, CA.
- Clech, J-P., "Lead-Free Solder Joint Reliability - Back To The Basics", Hobbs Engineering Webinar, March 18, 2015.
- Clech, J-P., "Lead Free Soldering and Joint Reliability: Fundamentals and Design-For-Reliability Rules", Chapter 63 in *Printed Circuits Handbook*, 7th Edition, ed. C. Coombs and H. Holden, McGraw-Hill Ryerson, 2016.
- Dai, X., Pan, N., Castro, A., Culler, J., Hussain, M., Lewis, R. and Michalka, T., "High I/O Glass Ceramic Package Pb-free BGA Interconnect Reliability", IEEE, Proceedings, ECTC 2005.
- Darveaux, R., Heckman, J. and Mawer, A., "Effect of test board design on the 2nd level reliability of a fine pitch BGA package", Proceedings, Surface Mount International Conference, August 25-27, 1998, San Jose, CA, pp. 105-111.
- De Vries, J., Jansen, M., Van Driel, W., "Solder-joint reliability of HVQFN-packages subjected to thermal cycling", *Microelectronics Reliability*, 2009, Vol. 49, pp. 331-339.
- Farooq, M., Goldman, L., Martin, G., Goldsmith, C. and Bergeron, C., "Thermo-mechanical fatigue reliability of Pb-free ceramic ball grid arrays: experimental data and lifetime prediction modeling", IEEE, Proceedings, ECTC 2003.
- Ghaffarian, R., "CSP reliability for single- and double-sided assemblies", *Chip Scale Review*, Vol. 3, No. 6, November / December 1999, pp. 34-39.
- Hall, P.M., "Forces, moments, and displacements during thermal chamber cycling of leadless ceramic chip carriers soldered to printed boards", *IEEE Transactions on Components, Hybrids and Manufacturing Technology*, 1984, Vol. 7, No. 4, Dec. 1984, pp. 314-327.
- IPC-9701, Performance Test Methods and Qualification Requirements for Surface Mount Solder Attachments.
- IPC-SM-785, Guidelines for Accelerated Reliability Testing of Surface Mount Solder Attachments.
- Juso, H., Yamaji, Y., Kimura, T., Fujita, K., Kada, M., "Board level reliability of CSP", IEEE, Proceedings, ECTC, May 25-28, 1998, Seattle, WA, pp. 525-531.
- Lau, J. H. and Lee, S-W. R., "Effects of Build-Up Printed Circuit Board Thickness on the Solder Joint Reliability of a Wafer Level Chip Scale Package (WLCSP)", *IEEE Transactions On Components And Packaging Technologies*, Vol. 25, No. 1, March 2002, pp. 3-14.
- Pendse, R., Afshari, B., Butel, N., Leibovitz, J., Hosoi, Y., Shimada, M., Maeda, K., Maeda, M. and Yonekura, H., "New CBGA Package with Improved 2nd Level Reliability", IEEE, Proceedings, ECTC 2000.
- Primavera, A., "Influence of PCB parameters on chip scale package assembly and reliability (Part I)", Proceedings of the Chip Scale Packaging Symposium, SMTA International, San Jose, CA, September 12-16, 1999, pp. 97-109.
- Primavera, A., "Predicting reliability of double-sided area array assemblies", *Circuits Assembly*, October 2003, pp. 22-26.
- Shih, R., Dai, S., Billaut, F., Teng, S., Hu, M. and Hubbard, K., "The effect of printed circuit board thickness and dual-sided configuration on the solder joint reliability of area array packages", IMAPS Conference, 2004.
- Shih, R., Dai, S., Ramos, N., Billaut, F., Gopalakrishnan, L., Hu, M., Hubbard, K., Teng, S., Lee-Kim, N., Besuk, S. and Imura, R., "Reliability of HITCE Ceramic Ball Grid Array Package", IMAPS Conference, 2005.
- Syed, A., Panczak, T., Darveaux, R., Lee, SG, Lee, CH, and Partridge, J., "Solder joint reliability of ChipArray BGA", *Journal of Surface Mount Technology*, April 1999, pp. 1-7.
- Teng, S. Y. and Brillhart M., "Reliability Assessment of a High CTE CBGA for High Availability Systems", IEEE, Proceedings, ECTC 2002.
- Vandevelde, B., Gonzalez, M., Beyne, E., Vandepitte, D. and Baelmans, M., "Influence of printed circuit board properties on solder joint fatigue life of assembled IC packages", European Microelectronics and Packaging Symposium, Prague, Czech Republic, June 16-18. 2004.
- Wu, K-C. and Chiang, K-N., "Investigation of Solder Creep Behavior on Wafer Level CSP Under Thermal Cycling Loading", Proceedings, IEEE, ICEP Conference, 2014, pp. 498-501.